Evaluation of a Follower Load with an Intact Rib Cage

By

Hadley L. Sis

Submitted to the graduate degree program in Bioengineering and the Graduate Faculty of the University of Kansas in partial fulfillment of the requirements for the degree of Master of Science.

_____
Chairperson Dr. Elizabeth Friis

_____
Dr. Ronald Dougherty

_____
Dr. Carl Luchies

Date Defended: December 3, 2015

The Thesis Chairperson for Hadley L. Sis

certifies that this is the approved version of the following thesis:

EVALUATION OF A FOLLOWER LOAD WITH AN INTACT RIB CAGE

_____

Chairperson Dr. Elizabeth Friis

Date approved: December 3, 2015

Abstract

The overall goal of this research was to better characterize the motion of the thoracic spine by inclusion of the rib cage and a novel loading method, as well as by evaluation of all commonly used motion and stiffness parameters.

Past researchers have reported on the importance of the rib cage in maintaining mechanical stability in the thoracic spine. However, because of inconsistencies in test machines and experimental design, the rib cage is often removed when testing the thoracic spine. Applying pure compressive loads to simulate muscle forces and body weight has proven difficult because of the natural curvature of the spine. Development of a follower load by previous researchers has improved upon this issue, allowing more physiologically representative loads to be used by applying the loads along the natural curvature of the spine. Most spine testing does not involve the thoracic spine, and of that research, even less involves the thoracic spine with an intact rib cage or compressive loads similar to that of thoracic musculature. Quantification of the motion of the thoracic spine with the rib cage and a follower load is important in order to provide the research and clinical spine communities with more relevant data that includes essential elements needed to obtain better characterization of the motion.

An *in vitro* biomechanical study of human cadaveric thoracic specimens with rib cage intact in lateral bending, flexion/extension, and axial rotation under varying compressive follower preloads was performed. The hypotheses tested for all modes of bending were (i) range of motion, elastic zone, and neutral zone will be reduced with a follower load, and (ii) neutral and elastic zone stiffnesses will be increased with a follower load. Eight human

cadaveric thoracic spine specimen (T1-T12) with intact rib cages were subjected to 5 Nm pure moments in lateral bending, flexion/extension, and axial rotation under follower loads of 0 to 600 N. Range of motion, elastic and neutral zones, and elastic and neutral zone stiffness values were calculated for functional spinal units and segments within the entire thoracic section.

Significance at various levels and for certain parameters varied, but overall, combined segmental range of motion decreased with follower load for every mode of bending. Based upon this experimentation, it is seen that application of a follower load with an intact rib cage does alter the motion and stiffness of the human cadaveric thoracic spine. Future researchers should consider including both of these aspects to better represent the physiologic implications of human motion and improve clinically relevant biomechanical thoracic spine testing. Recommendations for future testing in this area involve further characterization of the thoracic spine, including, but not limited to, the effect of the follower load on the thoracic spine without an intact rib cage, evaluation of the contribution of the free-floating ribs, and changes in intradiscal pressure with application of a follower load.

Abstract.....iii
Table of Contents.....v
List of Figures.....vi
List of Tables.....viii
Chapter 1. Introduction.....1
Chapter 2. Background.....3
2.1. Spine Anatomy.....3
2.2. Biomechanical Spine Testing.....4
2.3. Current Thoracic Spine Testing.....7
2.4. Test Machine.....8
2.5 Follower Load System.....10
2.6 References.....13
Chapter 3. Manuscript for Submission to JOR.....16
Title Page.....17
Abstract.....18
Keywords.....18
Introduction.....19
Materials and Methods.....20
Results.....22
Discussion.....23
Acknowledgements.....28
References.....29
Figures.....31
Tables.....38
Chapter 4. Conclusions and Future Work.....42
Appendix A: Data Analysis.....44
A.1 Data Analysis Parameter Calculations Matlab Code.....45

List of Figures

Chapter 2

Figure 1: Anatomy of the Spine (Public Domain)…….....3

Figure 2: Depiction of rotations and body planes as applied to two vertebral levels. Image reprinted with permission of Springer©……..4

Figure 3: Representation of the motion and stiffness parameters as taken from an angular displacement vs. load curve……..5

Figure 4: The FS20 Biomechanical Spine Testing System, demonstrating the placement of a specimen in relation to the machine set-up (Applied Test Systems).....9

Figure 5: Depiction of the way a compressive load acts on the spine (left figure) vs. the way the follower load instrumentation applies the load (right figure) (InnerBody.com)……..11

Chapter 3

Figure 1. Inferior view of the interior of the rib cage, displaying the ball joint rod ends and rods threaded through the approximate centers of each vertebrae, T3-T11. The wire cable, not pictured, was then threaded superior to inferior through all of the ball joint rod ends seen.....31

Figure 2. Sagittal view of the entire specimen, with the inferior potting mounted on the test machine. The motion tracking pins are shown at the various vertebral levels. The arrows refer to the steel wire cable, which is threaded from the superior end, through the ball joint rod ends on the interior of the rib cage, and out the inferior end of the specimen.....32

Figure 3. Deformation versus load of a typical testing cycle. The parameters of overall range of motion, elastic zone ROM, neutral zone ROM, EZ stiffness, and NZ stiffness are depicted…33

Figure 4. Mean combined segmental angular displacement range of motion values, displaying the difference between each load level and mode of bending.....34

Figure 5. Mean (+ SD) segmental angular displacement range of motion values for lateral bending, comparing the baseline case of 0 N to the two other load levels, 200 and 400 N. * denotes statistically significant values between 0-200 N and 0-400 N ($p < .05$) † denotes statistically significant values between 200-400 N ($p<.05$).....35

Figure 6. Mean (+ SD) individual FSU angular displacement range of motion values for lateral bending, comparing the baseline case of 0 N to the two other load levels, 200 and 400 N. * denotes statistically significant values between 0-200 N and 0-400 N ($p < .05$) † denotes statistically significant values between 200-400 N ($p<.05$)……36
Figure 7. Mean (+ SD) individual FSU angular displacement elastic zone values for lateral bending, comparing the baseline case of 0 N to the two other load levels, 200 and 400 N. * denotes statistically significant values between 0-200 N and 0-400 N ($p < .05$) † denotes statistically significant values between 200-400 N ($p<.05$).....37

List of Tables

Chapter 3

Table 1: Mean (SD) Angular Displacement Values for Individual FSU Range of Motion, Elastic Zone, and Neutral Zone……38

Table 2: Mean (SD) Angular Displacement Values for Segmental Range of Motion, Elastic Zone, and Neutral Zone……39

Table 3: Mean (SD) Stiffness Values for Individual FSU Elastic Zone Stiffness and Neutral Zone Stiffness……40

Table 4: Mean (SD) Stiffness Values for Segmental Elastic Zone Stiffness and Neutral Zone Stiffness……41

Chapter 1: Introduction

The purpose of this research was to better characterize the motion of the thoracic spine, by inclusion of the rib cage and application of a follower preload in cadaveric testing of this spine section.

Biomechanical spine testing is performed for the purpose of gaining more understanding of the physiological implications of the movement of the spine and implementation of current medical practices. Conclusions gathered regarding the efficacy of surgical techniques and devices are typically based on data from human cadaveric motion studies. Because these studies have such a large influence on the clinical community, the similarity of the methodology of said studies to normal human motion is of the utmost importance. The objective of this research was to combine a few biomechanical techniques commonly used individually in spine testing, in order to better characterize the natural motion of the thoracic spine and to provide the spine community with more relevant data pertaining to the motion of the thoracic spine.

Most spine testing does not involve the thoracic spine, and of that research, even less involves the thoracic spine with an intact rib cage or compressive loads similar to that of thoracic musculature. Information about the thoracic spine motion is sparse and does not involve all elements needed to fully characterize the motion.

The hypotheses presented in this study state that an applied load will affect the movement of the thoracic spine, specifically that the motion of the spine will decrease and the stiffness will increase.

The first chapter of this paper has provided the overall motivation and significance for this research study. The second chapter will focus on the background, establishing the knowledge necessary to understand this research. The third chapter is a manuscript currently submitted to a scientific journal, describing the entire study. The fourth and final chapter concludes the paper and discusses possible future work.

Chapter 2: Background

2.1 Spine Anatomy

The vertebrae, or the bones of the spine, serve as the hard elements of the spine, protect the spinal cord and nerves, and sustain compressive loads and facilitate motion [1]. Located in between each adjacent vertebrae is an intervertebral disc which acts as a cushion to distribute loads. Three distinct sections make up the spinal column: cervical, thoracic, and lumbar. These sections are shown in Figure 1. Seven cervical vertebrae make up the neck and provide the motion necessary for movement of the head. Twelve thoracic vertebrae make up the trunk section of the body, are connected to the ribs, and provide structural support. Five lumbar vertebrae make up the lower back and sustain the highest forces and motion of the entire spine. The cervical and lumbar sections of the spine follow a lordotic curvature, or one that is concave toward the back. The thoracic section has a kyphotic curve, or one that is convex toward the back.

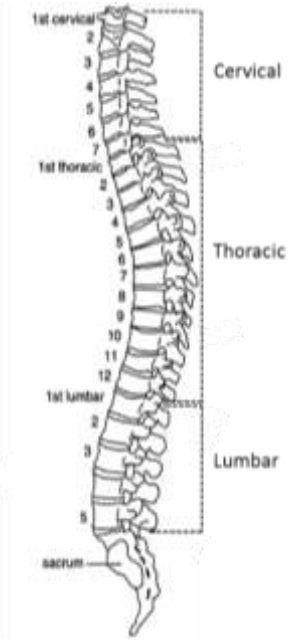

Figure 1: Anatomy of the Spine (Public Domain)

Functional spinal units (FSUs) are commonly examined during biomechanical spine testing. A FSU is comprised of any two adjacent vertebrae, the intervertebral disc between them, and all connecting musculature. It is commonly referred to as a single motion segment.

Three coupled kinematic motions are used to examine the motion of the spine. Flexion and extension, or forward and backward bending, take place in the frontal plane. Lateral bending, or right and left side bending, takes place in the sagittal plane. Axial rotation, or right and left twisting, takes place in the transverse plane. These bending planes, as they relate to motion of an individual vertebra, are shown in Figure 2.

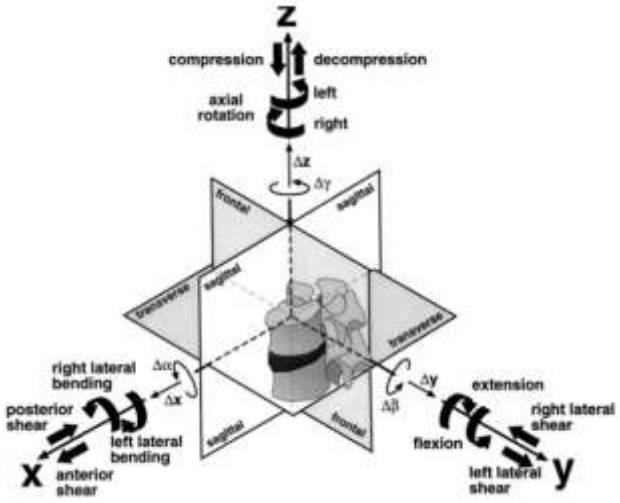

Figure 2: Depiction of rotations and body planes as applied to two vertebral levels.

Image reprinted with permission of Springer©

2.2 Biomechanical Spine Testing

Biomechanical testing of the spine has been performed by many researchers, in an attempt to better understand the physiological implications of surgical techniques and device design. Panjabi et al. first began the discussion about the proper procedures for testing the human

spine, and Wilke et al. standardized the proper protocol for such testing, including test setup, definition of coordinate systems, and the parameters to be calculated from the resultant data [2-3]. Testing is typically performed in the three modes of bending: lateral bending, flexion/extension, and axial rotation, on FSUs. The main parameters examined in this testing, and depicted in Figure 3, are:

- Range of motion (ROM): the sum of the neutral zone and the elastic zone in one direction of motion
- Elastic zone (EZ): the deformation measured from the end of the neutral zone to the point of maximal loading
- Neutral zone (NZ): the difference in angulation at zero load or the range over which the specimen moves essentially free of applied loading
- Elastic zone stiffness (EZS): the stiffness characterizing the elastic deformation of the specimen
- Neutral zone stiffness (NZS): the stiffness characterizing the relatively lax deformation of the specimen or the quotient of the loading to the deformation

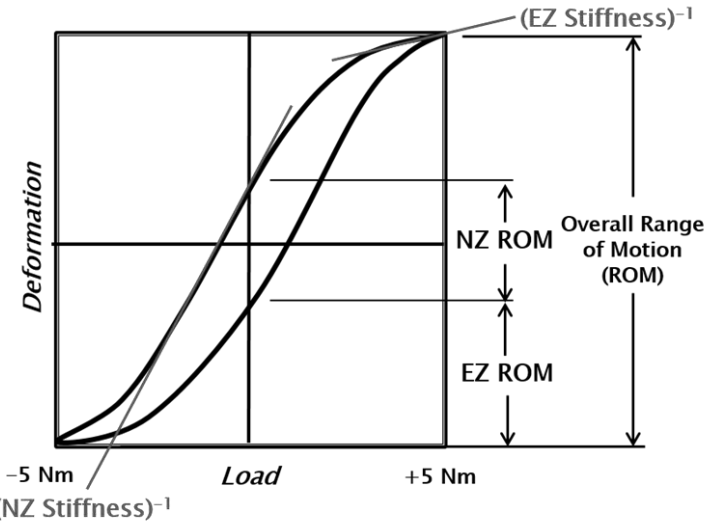

Figure 3: Representation of the motion and stiffness parameters as taken from an angular displacement vs. load curve

Recent spine research has made an effort to include most of these parameters, but due to data collection and methodology limitations, most past spine research only focuses on overall ROM. Motion in the neutral zone is caused only by passive motion, or motion where only the spinal column is contributing and it is offering little resistance [4]. The elastic zone motion has contributions from both the soft and hard tissues of the spine, meaning activation of the spinal muscles is occurring. Panjabi has expressed the clinical importance of the NZ and NZS parameters, as this region correlates strongly with patient pain in the spine [5]. Stiffness parameters correspond directly with the stability of the spine, as defined by Pope and Panjabi [6]. Because of the clinical relevance of these motion and stiffness parameters, all five of them are beneficial to examine when performing tests of this nature.

Most spine testing analysis is performed using the projection method and Euler method as defined by previous researchers [7]. Each vertebra being examined is assigned its own local coordinate system based upon anatomical points on the vertebra, which can then be related to

adjacent vertebrae, or a vertebra at the end of a segment. Motion of each vertebra being tracked is calculated relative to another vertebra being tracked [8]. The method of applying a coordinate system to each vertebra has been the standard in this field of testing. Load versus displacement curves are gathered for every time point during every cycle for every vertebra, and the parameters previously stated are computed from these curves. Appendix A contains information about the specific parameter calculations.

Some statistical analyses in the field of spine biomechanics do not use correction factors when reporting alpha values, as the need for adjustment and the methods for correction remain unclear [9-10]. The majority of *in vitro* spine studies have very low statistical power, and some researchers have found that the use of corrections can increase the chance of Type II error. This heightened possibility of Type II error can be detrimental to the observation of significance or trends in such small sample sizes. A correction factor was not used in the statistical analysis of the current study in order to take a less conservative approach and to observe as many trends as possible for the practical understanding of the data.

The majority of *in vitro* spine testing data is presented for individual FSUs [3]. This is due to the prevalence of individual levels when patients are experiencing pain and, consequently, the correction of said pain. Motion of individual FSUs is important for clinicians when examining how a surgical technique or implant will alter a patient's everyday motion. On the other hand, *in vivo* spine testing data is often presented by segments, or multiple vertebral levels, instead of one FSU level. This is due to testing methodology limitations when dealing with living subjects because of skin or fatty tissue, as well as the prevalence of this data in the physical therapy community, where pain is treated by larger segments of the spine, such as the neck or lower

back [11]. Data in this study is presented in both formats, in an effort to glean comparisons between other *in vivo* and *in vitro* work.

2.3 Current Thoracic Spine Testing

The thoracic spine is vastly different from the other sections because of the presence of the rib cage. Due to size constraints of typical biomechanical test machines, thoracic spine research has not typically involved keeping the rib cage intact. However, researchers have reported on the importance of maintaining the structure of the rib cage, as it greatly impacts the motion and stability of the thoracic spine [12-17]. Watkins et al. discovered more than a 30% contribution on average to overall thoracic stiffness when examining the rib cage effect on stability of the entire thoracic section [14]. Brasiliense et al. used segments comprised of four vertebral levels with the corresponding levels of the rib cage intact, and reported that the rib cage contributed 78% to the overall stability for each segment [15]. A significant 77% increase in thoracic range of motion was reported by both Mannen et al. and Oda et al. when examining the difference between motion of a thoracic spine section with and without a rib cage [16-17].

The thoracic spine has been tested much less frequently than the lumbar and cervical spines, due to the size of the section and the presence of the rib cage. While the cervical and lumbar spine sections are associated more often with pain during motion than the thoracic spine, researchers have validated the necessity to characterize the motion of the thoracic section [3, 18-20]. Nicoll et al. found that wedge-shaped fractures of a vertebral body can create greater moment arms and bending moments in the spine, producing enlarged kyphotic deformity and pressure on the spinal cord [21]. This issue is particularly prevalent in the already

kyphotic thoracic spine, and thus, a fracture in this spinal section can potentially produce more deformity and instability than a fracture in the other spinal sections. It has also been found that the frequency of vertebral fractures in the thoracic section is very similar to that of the lumbar section [22]. Because of this prevalence of injury in the thoracic spine, the lack of information about this spinal region needs to be improved upon.

2.4 Test Machine

Types of testing machines vary widely in the field of biomechanical spine testing, ranging from manual set-ups to automated machines. Manual testing methodology involves the use of pulley-and-weight systems to discretely apply a load to a specimen. User error and repeatability are issues with this testing. Automated machines use continual loading techniques and are usually repurposed industrial robotic apparatuses. An issue with these machines is that they are not typically validated using any standard procedures to ensure accuracy of results. Despite the inconsistencies sometimes seen with current automated test machines, testing with continuous motion has proven to be much more beneficial and accurate than manual testing [23]

The testing apparatus used in this research, a FS20 Biomechanical Spine Test System, was designed by ATS (Applied Test Systems, Butler, PA). It was validated in a subsequent study by Mannen et al. [24]. A picture of the test machine is shown in Figure 4. The machine allows for testing of all three spine regions in all modes of bending, including the entire thoracic region with rib cage intact. It applies pure bending moments and can be either load- or displacement-controlled. Two arms regulate the motion of the specimen on the platform, one that performs

in-plane bending (lateral bending and flexion/extension), and one that performs torsion (axial rotation). The machine works in tandem with an external motion tracking system, synchronizing the motion of a specimen with the load being applied. Orthopedic research pins communicating with an Optotrak motion tracking system were used in tandem with the test machine in the current study.

Figure 4: The FS20 Biomechanical Spine Testing System, demonstrating the placement of a specimen in relation to the machine set-up (Applied Test Systems)

2.5 Follower Load System

Application of compressive loads in spine testing has been done by previous researchers, in order to mimic forces of body weight and musculature on the spine. The erector spinae muscle group provides the majority of the stability for the thoracic spine, and the forces of these muscles greatly impact the motion of the spinal region [1]. However, achieving high loads when testing an entire region of the spine has been difficult because of the curved nature

of the spinal regions. Simple compressive loads applied superior to the spinal region cause premature buckling of the column. Patwardhan et al. developed a novel loading technique that applies a load which follows the natural curve of the spine, allowing the load to be applied in a manner more similar to the actual loading of the human spine [25]. This technique has been applied in subsequent studies and has been shown to increase the load-carrying capacity of the lumbar, cervical, and thoracolumbar spine regions, allowing more physiologically representative weights to be applied when testing [26-28]. Range of motion was seen to significantly decrease with an increase in load in all of the previously stated spine studies. Other researchers have been successful when reproducing the follower preload in subsequent studies. Tawackoli et al. demonstrated the efficacy of the follower load in the thoracolumbar spine (T9-L3) with loads up to 975 Newtons, and found decreased bending flexibility in the spine with this increasing load level [29].

The overarching idea of a follower preload is that the load is applied approximately tangent to the curve of the spine, such that each vertebral body is loaded in near pure compression. This differs from a simple compressive load which is applied to the first vertebral body, distributing the weight directly perpendicular to the ground, not along the curve of the spine. When weight is applied in this compressive manner to a multilevel spine segment, buckling occurs at much smaller loads than the segment should normally be capable of withstanding. This increase in load-carrying capacity of the spinal segment is important during biomechanical testing, as it allows forces to be applied which would represent *in vivo* muscle forces and the weight of the upper body. A representation of the differences between these methods is shown in Figure 5.

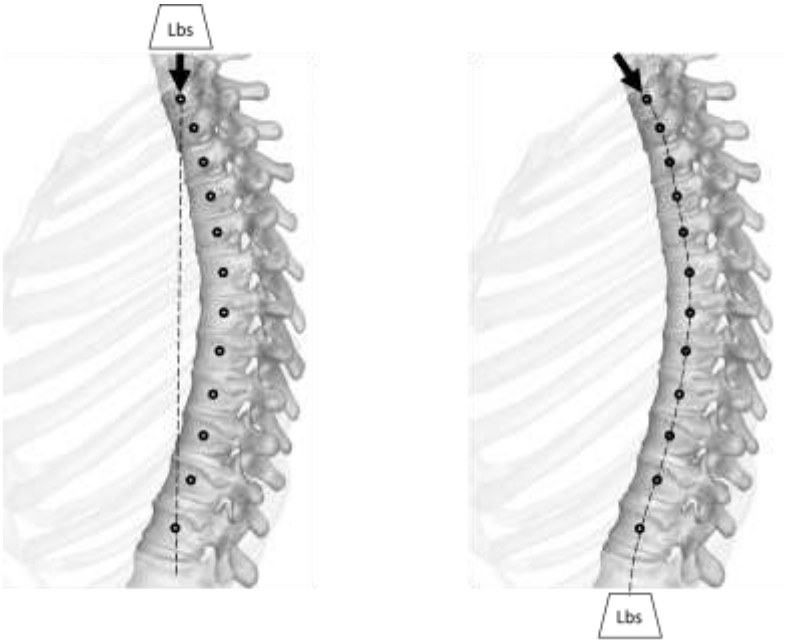

Figure 5: Depiction of the way a compressive load acts on the spine (left figure) vs. the way the follower load instrumentation applies the load (right figure) (InnerBody.com)

The level of follower load applied in studies varies greatly by which spine section is being examined. A 250 N load limit has been used in the cervical spine (C1-C7), an 800 N limit has been applied in the thoracolumbar spine (T2-sacrum), and a 1200 N load has been used in the lumbar spine (L1-sacrum) [26-28]. A 975 N load has been successfully implemented in a partial thoracolumbar spine (T9-L3) [29]. Based upon these previously evaluated limits, a load of 600 N was originally chosen to be the maximum load used for this work. Although not much data is available on the actual percent contribution of total muscle effort and load bearing of each spinal section, the thoracic spine was seen to be in the middle ground between the lowest and highest follower loads applied in the cervical and lumbar sections, respectively. Incremental loading in 200 N stages, beginning with 0 N, has been utilized in past research in

order to simulate the range of minimal to moderate muscle effort, and was also applied to the current work [25].

The follower load instrumentation used in the current study needed to be modified in order to achieve implementation with the rib cage intact. The spatial constraints of the intact specimen provided some difficulty in mimicking the design used by previous researchers. The method used to apply the instrumentation to the vertebral bodies with the rib cage intact was deemed appropriately similar to the test setup seen in previous studies, and it successfully allowed the load to run bilaterally to each vertebra.

2.6 References

1. Kurtz S. M., and Edidin A. 2005. Spine Technology Handbook. Burlington: Elsevier Inc.
2. Panjabi M. M., Krag M. H., and Goel V. K. 1981. A technique for measurement and description of three-dimensional six degree-of-freedom motion of a body joint with an application to the human spine. J Biomech 14: 447-460.
3. Wilke H., Wenger K., Claes L. 1998. Testing criteria for spinal implants: recommendations for the standardization of in vitro stability testing of spinal implants. Eur Spine J 7: 148-54.
4. White A., Panjabi M. 1990. Clinical Biomechanics of the Spine, 2nd ed. Philadelphia: Lippincott Williams & Wilkins; 722 p.
5. Panjabi M. 2003. Clinical spinal instability and low back pain. J Electromyogr Kines 13: 371-79.
6. Pope M., Panjabi M. 1985. Biomechanical definitions of spinal instability. Spine 10: 255-56.
7. Crawford N. R., Yamaguchi G. T., Dickman C. A. 1996. Methods for determining spinal flexion/extension, lateral bending, and axial rotation from marker coordinate data: analysis and refinement. Human Movement Science 15: 55-78.
8. Wilke H. J., Jungkunz B., Wenger K., et al. 1998. Spinal segment range of motion as a function of in vitro test conditions: effects of exposure period, accumulated cycles, angular-deformation rate, and moisture condition. The Anatomical Record 25: 15-19.
9. Perneger T. What's wrong with Bonferroni adjustments? 1998. Br Med J 316:1236–8.
10. Nakagawa S. 2004. A farewell to Bonferroni: the problems of low statistical power and publication bias. Behav Ecol 15(6):1044–5.
11. Menegoni F., Vismara L., Capodaglio P., et al. 2008. Kinematics of trunk movements: protocol design and application in obese females. J Appl Biomater Biom 6: 178-85.
12. Healy A. T., Lubelski D., Mageswaran P. 2014. Biomechanical analysis of the upper thoracic spine after decompressive procedures. The Spine Journal 14: 1010-1016.
13. Oda I., Abumi K., Cunningham B., et al. 2002. An *in vitro* human cadaveric study investigating the biomechanical properties of the thoracic spine. Spine 27: E64-E70.

14. Watkins R.T., Watkins R. III, William L., et al. 2005. Stability provided by the sternum and rib cage in the thoracic spine. Spine 30: 1283-6.
15. Brasiliense L., Lazaro B., Reyes P., et al. 2011. Biomechanical contribution of the rib cage to thoracic stability, Spine 36: E1686-93.
16. Mannen E., Anderson J., Arnold P., et al. 2015. Mechanical contribution of the rib cage in the human thoracic cadaveric thoracic spine. Spine 40: 1-7.
17. Oda I., Abumi K., Lu D., et al. 1996. Biomechanical role of the posterior elements, costovertebral joints, and rib cage in the stability of the thoracic spine. Spine 21: 1423–1429.
18. Andersen J.H., Haahr J.P., Frost P. 2007. Risk factors for more severe regional musculoskeletal symptoms: a two-year prospective study of a general working population. Arthritis and rheumatism 56: 1355-1364.
19. Delmas P.D., van de Langerijt L., Watts N.B., et al. 2005. Underdiagnosis of vertebral fractures is a worldwide problem: the IMPACT study. Journal of Bone and Mineral Research 20: 557-563.
20. Melton L.J., Lane A.W., Cooper C., et al. 1993. Prevalence and incidence of vertebral deformities. Osteoporosis international : a journal established as result of cooperation between the European Foundation for Osteoporosis and the National Osteoporosis Foundation of the USA 3: 113-119.
21. Nicoll E. 1949. Fractures of the dorso-lumbar spine. J Bone Joint Surg 31: 376.
22. Cooper C., Atkinson E., O'Fallon M., et al. 1992. Incidence of clinically diagnosed vertebral fractures: a population-based study in Rochester, Minnesota, 1985-1989. J Bone Miner Res 7.
23. Goertzen D. J., Lane C., and Oxland T. R. 2004, "Neutral zone and range of motion in the spine are greater with stepwise loading than with a continuous loading protocol. An in vitro porcine investigation," J Biomech, 37(2): 257-261.
24. Mannen E., Ranu S., Villanueva A., et al. 2015. Validation of a novel spine test machine. J Med Devices 9.

25. Patwardhan A., Havey R., Meade K., et al. 1999. A follower load increases the load-carrying capacity of the lumbar spine in compression. Spine 24: 1003-9.

26. Patwardhan A., Havey R., Carandang G., et al. 2003. Effect of compressive follower preload on the flexion-extension response of the human lumbar spine. Journal of Orthopedic Research 21: 540-546.

27. Patwardhan A., Havey R., Ghanayem A., et al. 2000. Load-carrying capacity of the human cervical spine in compression is increased under a follower load. Spine 25: 1548-54.

28. Stanley S., Ghanayem A., Voronov L., et al. 2004. Flexion-extension response of the thoracolumbar spine under compressive follower preload. Spine 29: E510-14.

29. Tawackoli W., Marco R., Liebschner M. 2004. The effect of compressive axial preload on the flexibility of the thoracolumbar spine. Spine 29: 988-993.

Chapter 3: Manuscript for Submission to JOR

The following contains a manuscript submitted on November 6th, 2015 to the Journal of Orthopedic Research. It has been vetted and approved by all co-authors prior to submission. Hadley Sis had significant contribution to the experimental design, follower load design, data collection, data analysis, and data publication.

Effect of a Follower Load on the Motion and Stiffness of a Human Cadaveric Thoracic Spine with an Intact Rib Cage

Effect of Follower Load on Motion and Stiffness of the Human Thoracic Spine with Intact Rib Cage

Hadley L. Sis
The University of Kansas, Bioengineering Program, Lawrence, KS, USA
1530 W 15th St., Learned Hall Room 3135A, Lawrence, KS, 66045
hadley.sis@ku.edu

Erin M. Mannen
The University of Kansas, Department of Mechanical Engineering, Lawrence, KS, USA
1530 W 15th St., Learned Hall Room 3138, Lawrence, KS 66045
erinmannen@gmail.com
Substantial contributions to research design, critical revision, and approval of final version

Benjamin M. Wong
The University of Kansas, Bioengineering Program, Lawrence, KS, USA
1530 W 15th St., Learned Hall Room 3135A, Lawrence, KS, 66045
benjamin.m.wong@ku.edu
Substantial contributions to research design, critical revision, and approval of final version

Eileen S. Cadel
The University of Kansas, Bioengineering Program, Lawrence, KS, USA
1530 W 15th St., Learned Hall Room 3135A, Lawrence, KS, 66045
ecadel@ku.edu
Substantial contributions to research design, critical revision, and approval of final version

Mary L. Bouxsein
Beth Israel Deaconess Center, Harvard Medical School, Boston, MA, USA
330 Brookline Ave, RN 115, Boston, MA, 02215
mbouxsei@bidmc.harvard.edu
Substantial contributions to research design, critical revision and approval of final version

Dennis E. Anderson
Beth Israel Deaconess Center, Harvard Medical School, Boston, MA, USA
330 Brookline Ave, RN 115, Boston, MA, 02215
danders7@bidmc.harvard.edu
Substantial contributions to research design, critical revision, and approval of final version

Elizabeth A. Friis[1]
The University of Kansas, Department of Mechanical Engineering, Lawrence, KS, USA
1530 W 15th St., Learned Hall Room 3138, Lawrence, KS 66045
(785) 864-2104
lfriis@ku.edu
Substantial contributions to research design, critical revision, and approval of final version

Abstract

Researchers have reported on the importance of the rib cage in maintaining mechanical stability in the thoracic spine and on the validity of a compressive follower preload. However, mechanical testing using both the rib cage and follower load has never been studied. An *in vitro* biomechanical study was performed on human cadaveric thoracic specimens with rib cage intact in lateral bending, flexion/extension, and axial rotation under varying compressive follower preloads. The objective was to characterize the motion and stiffness of the thoracic spine with intact rib cage and follower preload. The hypotheses tested for all modes of bending were (i) range of motion, elastic zone, and neutral zone will be reduced with a follower load, and (ii) neutral and elastic zone stiffness will be increased with a follower load. Eight human cadaveric thoracic spine specimen (T1-T12) with intact rib cages were subjected to 5 Nm pure moments in lateral bending, flexion/extension, and axial rotation under follower loads of 0 to 600 N. Range of motion, elastic and neutral zones, and elastic and neutral zone stiffness values were calculated for functional spinal units and segments within the entire thoracic section. Combined segmental range of motion decreased with follower load for all three modes of bending. Application of a follower load with an intact rib cage impacts the motion and stiffness of the human cadaveric thoracic spine, particularly in lateral bending and axial rotation. Researchers should consider including both of these aspects to better represent the physiologic implications of human motion and thus improve clinically relevant biomechanical thoracic spine testing.

Key Words:

thoracic spine; rib cage; follower load; biomechanics

1. Introduction

The kyphotic nature of the thoracic spine and the presence of the rib cage create a unique mechanical phenomenon in the middle spinal section that is not fully understood. Biomechanical testing of the thoracic spine provides necessary information for evaluation of instability in the spine and for creation of new treatment methods and improved device design. Previous research has reported the importance of the rib cage in maintaining mechanical stability in the thoracic spine. Watkins et al. used the full thoracic section (T1-T12) to examine effects of the rib cage on thoracic spine stability, and found more than a 30% contribution to overall thoracic stiffness in all three modes of bending [1]. In another study, Brasiliense et al. reported that the rib cage contributed, on average, 78% of the overall thoracic stability [2]. This influence was confirmed by Mannen et al., who reported a 77% increase in the overall thoracic range of motion in axial rotation with the rib cage removed [3]. These findings provide unanimous agreement that rib cage removal when performing mechanical testing of the thoracic spine is not indicative of the physiological stability present in the thoracic skeleton. However, these studies did not use a compressive follower preload with the rib cage attached.

Because the spine operates under compressive conditions *in vivo,* researchers have reported on the use of a follower load to simulate this condition during mechanical testing in other sections of the spine. As defined by Patwardhan et al., a follower load applies the compressive preload approximately tangent to the curve of the spine, passing through the centers of rotation of the spinal segments [4]. Conversely, direct compressive loading does not follow the curvature of the spine and can cause buckling in multilevel spine segments. A compressive follower preload allows each individual vertebra to be loaded in nearly pure compression. Patwardhan et al. initially found a high increase in load-carrying capacity of the lumbar spine

under compressive follower loads relative to direct loading, and proved this finding for the cervical and thoracolumbar spinal segments in subsequent studies [4-6]. This increase in load-carrying capacity corresponds to the ability of these spinal segments to support *in vivo* muscle forces and the weight of the upper body with engagement of ligaments and other essential tissues. The muscle forces present in the thoracic spine revolve around the erector spinae muscle group, which provides the majority of the stability to the thoracic spine.

The purpose of this study was to implement a compressive follower load on the thoracic spine with an intact rib cage, and examine the effects of the follower load on the *in vitro* range of motion and stiffness of the thoracic spine with rib cage intact. Motions of both individual functional spinal units (FSUs) and spinal segments within the entire thoracic spine were examined. FSUs consist of two adjacent vertebrae and all interconnecting soft tissues. The spinal segments were defined as upper (T1-T4), middle (T4-T8), and lower (T8-T12). The following hypotheses were tested through the course of this experiment: for individual FSUs and segments in all modes of bending, (i) range of motion (ROM), elastic zone (EZ), and neutral zone (NZ) will be significantly reduced with an increase in applied follower load, and (ii) neutral and elastic zone stiffness (NZS and EZS) will be significantly larger with an increase in applied follower load.

2. Materials and Methods

2.1 Experimental Design

Eight fresh-frozen adult human thoracic cadaveric spines (T1-T12) were used in this study, four male and four female. Average age was 66.9 ± 4.4 years. The specimens were dissected to include the rib cage, spinal column, and stabilizing ligamentous structures. Muscular and fatty tissues were removed. Specimens were thawed prior to testing and experiments were

performed at room temperature. Hydration of the specimens was maintained with a saline solution.

T1 and T12 were potted parallel to their vertebral endplates with screws inserted into the vertebral bodies and auto body filler (Bondo, 3M, St. Paul, MN). Bolts were rigidly fixed to the inferior potting and mounted on a FS20 Biomechanical Spine Test System (Applied Test Systems, Butler, PA) that allows 6 degrees-of-freedom with a pure continuous moment applied to the unconstrained, superior end (T1) [7]. The pure moment was applied at a 1 degree/second rate with a displacement control of +/- 5 Nm in three modes of bending: lateral bending, flexion/extension, and axial rotation. Five cycles were run for each test, with the third cycle used for data analysis. The motion of T1, T2, T4, T5, T8, T9, and T11 vertebrae were tracked using orthopaedic research pins (Optotrak, Northern Digital Inc., Waterloo, Ontario, Canada) rigidly fixed into the left pedicles. The FSU and segment levels chosen were reasonably spaced throughout the thoracic spine, producing representative motions of the top, middle, and bottom of the spine. Motion data from all seven pins and load data from the test machine were recorded.

2.2 Follower Load Implementation

Follower load instrumentation was based on the methods reported by Patwardhan et al. [4]. Modifications were made to account for the space-limiting presence of the rib cage. Fully-threaded steel rods were inserted into the approximate middle of the vertebral bodies of T3 through T11. Ball joint rod ends were screwed on both ends of all threaded rods, as shown in Figure 1. A steel wire cable was guided through the ball joint rod ends bilaterally. The top of the cable was threaded through the superior end of the potting, distributing the weight of the follower load from T1 to T11. The two bottom ends of the cable passed through pulleys to mimic the lordosis of the lumbar section and round out the spinal curve. Weights were hung from the

knotted ends of the cable. The total load was applied bilaterally in 200 N increments, ranging from 0 to 600 N. Figure 2 shows the experimental setup with the specimen mounted on the machine.

2.3 Data Analysis and Statistics

Data analysis and statistics were performed in Matlab (Mathworks, Natick, MA). Rotations were calculated using Euler decomposition techniques. For all modes of bending (lateral bending, flexion, extension, and axial rotation), ROM, EZ, NZ, EZS, and NZS were computed [8]. These parameters are depicted in Figure 3. Only four specimens were tested at a 600 N follower load due to concern for specimen integrity. Therefore, follower loads of 0, 200, and 400 N were included in the analyses. Comparisons were drawn between the baseline case (0 N) and each level of follower load applied (200 N and 400 N), as well as between the two levels of load applied. A one-way repeated measures analysis of variance (ANOVA) was completed with a significance level of 0.05. No correction factor was used as the methods for correction and the need for adjustment remain controversial [9-10].

3. Results

The combined segmental absolute value of ROM for all modes of bending is shown in Figure 4. This figure demonstrates the trend in ROM as the follower load increases. However, not all specific segment or FSU changes were found to be statistically significant. Segment and FSU data for lateral bending ROM are shown in detail in Figures 5 and 6 because of the large number of significant differences seen ($p < 0.05$). Compared to the 0 N load, segmental lateral bending ROM decreased by an average of 62.4% for a 200 N follower load, and by an average of 75.9% for a 400 N follower load. Compared to the 0 N load, FSU lateral bending ROM decreased by an average of 61.7% for a 200 N follower load, and by an average of 72.3% for a

400 N follower load. Significant decreases in EZ measurements were seen at every FSU level for lateral bending except T1/T2, as shown in Figure 7 ($p < 0.05$). Compared to the 0 N load, the EZ in lateral bending for all FSU levels decreased by an average of 64.5% for a 200 N follower load, and by an average of 75.6% for a 400 N follower load. Table 1 and Table 2 display all ROM, EZ, and NZ values for all modes of bending of FSUs and segments, respectively. Significance was seen for every FSU and segment of lateral bending ROM in at least one follower load comparison.

All stiffness values for all conditions of FSUs and segments are displayed in Table 3 and Table 4, respectively. Significant increases in NZS values were seen in the lower FSU and segment for lateral bending for all follower load comparisons. Significant differences were seen in NZS for axial rotation at the T4/T5, T8/T9, and T11/T12 levels, along with the lower segment.

Statistical significance was found for NZ at the T1/T2 level for lateral bending, for both load comparisons. Very little significance was found in EZS for any mode of bending, and the significance seen appeared randomly. Significance was seen at every segment for flexion ROM for at least one follower load comparison.

4. Discussion

As hypothesized, lateral bending ROM significantly decreased for segments and FSUs with an increase in follower load. However, statistically significant results for ROM were not consistent in segments and FSUs for axial rotation and flexion/extension. Also as hypothesized, various FSUs in axial rotation saw a significant increase in NZS with an increase in follower load, while stiffness values in other modes of bending produced inconclusive statistical results.

Range of Motion and Neutral Zone

The results of this study show that there was an effect on range of motion and stiffness in some modes of bending with a follower load, which is consistent with previous research that a follower preload is seen to have an effect on the loading capabilities of the spine. Although no rib cage was used, the 2004 thoracolumbar study by Stanley et al. relates closely to the overarching goals of this research, paving the way for application of a follower load on the thoracic section of the spine [6].

Direct comparisons between this study and past research were not possible, as no other studies have examined the same parameters at these anatomical levels with an intact rib cage and a follower preload. However, some trend comparisons can still be drawn between this study and others. In the study by Stanley et al., there was a decrease in ROM with a follower load for T2-T11 in flexion-extension, which is similar to the trend seen in the present study. Figure 4 clearly demonstrates this trend of decreasing overall combined range of motion with an increase in follower load, although not all ROM values were statistically significant. The absence of a significant difference could be because of the limited flexibility inherent in the thoracic section of the spine due to the presence of the rib cage, the mechanics of the facets, and/or the overlapping spinous processes [11]. Oda et al. has reported on ROM and NZ values for the canine thoracic spine with intact rib cage from T5-T8, relating most closely with the middle segment (T4-T8) tested in the current study with no follower load [12]. The same trends in average NZ values is seen in both studies, with lateral bending having the largest NZ and flexion/extension having the smallest NZ.

The significant differences found in the NZ measurements, particularly in lateral bending, are interesting, as NZ relates to the laxity of the specimen. Other research in this area has been inconclusive when looking for a significant decrease in NZ; however, it was seen at quite a few

levels in multiple modes of bending in the current study [13]. Panjabi indicated that an increase in NZ relates to an increase in pain, forcing the spine to overcompensate with increased activation of muscles and other internal stiffening methods [14]. Because of this pain relationship and the mechanical impact it has on the body, the statistically significant impact seen in the current study of follower load on NZ is important to note.

Neutral Zone Stiffness and Elastic Zone Stiffness

Because stability is an important factor in the clinical community, biomechanical test methods that affect stability should be considered. Pope has described instability in the spine as a loss of stiffness [15]. Based on this definition, the various statistically significant increases in NZS for some FSUs in lateral bending and axial rotation with a follower load could be indicative of an increase in mechanical stability. This implies that application of a follower load is important when assessing stability in spine testing.

More statistically significant increases in stiffness are most likely not present due to the large influence that the rib cage itself has on thoracic stiffness [16]. Various researchers have reported on the statistically significant decrease in overall stiffness that is seen with and without a rib cage [1, 3]. Future work should be performed by testing the thoracic spine without the rib cage in tandem with the follower load used in the current study, in order to further address this relationship of stiffness with and without the rib cage.

Some individual EZS and NZS values were much larger than others found within the same category, causing a high standard deviation. The variance in data seen at a particular FSU or segment level is the result of some specimens having much different magnitudes of stiffness as compared to the mean. Having wide variations between specimens is not unusual in this type

of testing. Future work in this area should explore test protocols that allow for more normalization between specimens used, in order to cut down on these kind of deviations.

Study Considerations

While there is not currently a standard procedure for applying a follower load in the thoracic section with the rib cage intact, this study successfully demonstrated that the technique can be applied in this context, as the specimens were able to withstand the large loads without noticeable tissue damage. With the presence of the rib cage, some of the instrumentation utilized in the protocols of the previous studies was not translatable to the current study because of lack of physical space for access to the vertebral bodies. The methods employed in this study were based upon reasonable alterations of the previously used method by Patwardhan et al. [4].

In previous literature, follower load levels have varied based on the spinal section being studied. A 250 N load limit has been applied to the cervical spine, an 800 N limit applied to the thoracolumbar spine, and a 1200 N limit applied to the lumbar spine [4-6]. Using these limits, a follower load of 600 N was originally chosen for the thoracic spine in this study, applied in increments of 200 N. The loading was completed in increments to simulate the range of minimal to moderate muscle effort [5]. As stated in the Methods section of this paper, only four specimens were tested at 600 N out of concern for specimen integrity. The use of small statured specimens in this study was, most likely, the largest influence for deviation from the expected threshold. However, all specimens did sustain a 400 N compressive follower preload without noticeable tissue damage. The cause of the large discrepancy between the 400 N load level in this study compared to the 800 N load level in Stanley et al.'s thoracolumbar study without the rib cage is unclear and should be researched further [6]. This could be completed by repeating

the current study's methodology with the rib cage removed, in order to better mimic the Stanley et al. study.

As with all experimental testing, issues, such as out-of-bounds sensors and low motion values, occurred in this study. Exclusion criteria were generated for range of motion and stiffness values, and applied to the resultant data. Due to these exclusions, various FSU and segment levels at some loads had 4 or fewer specimens contributing to the average value. Data gathered from these levels was not presented because of the small sample size, and are notated by a dash in the data tables.

It is important to understand the biomechanical behavior of individual levels and segments of the thoracic spine because of the large incidence rate of vertebral fractures occurring in the middle and lower thoracic sections, frequently occurring with little or no trauma [17]. Findings in previous *in vitro* research have centered on the analysis of individual FSUs [8]. This trend is due to the clinical relevance of FSUs in patient diagnosis and invasive treatment, as back pain and diseases are typically attributed to disc and facet issues at a specific vertebral level. Conversely, typical *in vivo* human motion research focuses on segmental analysis because of the desire for examining motion patterns in separate sections of the overall spine [18]. Segmental analysis is a clinically relevant ideology and is as beneficial and translatable to patient treatment as the commonly used FSU analysis. Because of the desire to normalize the two fields of cadaveric and human motion spine testing, future work should be done to compare values found in cadaveric spine studies to those found in human motion spine studies. Finding a relationship between these two testing methods could give significant insight into the field of spine testing.

It is noted that the distribution of force from the follower load is not identical to physiologic loading of the thoracic spine. In order to better mimic physiologic loading, different

sections of the thoracic spine should ideally carry varying weights and the load levels used should be based on a percentage of the body weight of the individual specimen. This study, however, presented a loading method that is similar to the protocols presented in past research.

Application of a follower load with an intact rib cage does impact the motion and stiffness of the human cadaveric thoracic spine. Future work in this area should include both a follower load and the intact rib cage in order to better represent the physiologic implications of human motion and improve clinically relevant biomechanical testing.

Acknowledgments:

This study was supported by the National Institute on Aging (K99AG042458) and by a Mentored Career Development Award from the American Society for Bone and Mineral Research (DEA). The authors state that they have no conflict of interest to disclose. The content is solely the responsibility of the authors and does not necessarily represent the official views of the National Institutes of Health. The authors thank Nikki Galvis for her help in dissections and testing.

References

1. Watkins R. T., Watkins R. III, William L., et al. 2005. Stability provided by the sternum and rib cage in the thoracic spine. Spine 30: 1283-6.

2. Brasiliense L., Lazaro B., Reyes P., et al. 2011. Biomechanical contribution of the rib cage to thoracic stability, Spine 36: E1686-93.

3. Mannen E., Anderson J., Arnold P., et al. 2015. Mechanical contribution of the rib cage in the human thoracic cadaveric thoracic spine. Spine 40: 1-7.

4. Patwardhan A., Havey R., Meade K., et al. 1999. A follower load increases the load-carrying capacity of the lumbar spine in compression. Spine 24: 1003-9.

5. Patwardhan A., Havey R., Ghanayem A., et al. 2000. Load-carrying capacity of the human cervical spine in compression is increased under a follower load. Spine 25: 1548-54.

6. Stanley S., Ghanayem A., Voronov L., et al. 2004. Flexion-extension response of the thoracolumbar spine under compressive follower preload. Spine 29: E510-14.

7. Mannen E., Ranu S., Villanueva A., et al. 2015. Validation of a novel spine test machine. J Med Devices 9.

8. Wilke H., Wenger K., Claes L. 1998. Testing criteria for spinal implants: recommendations for the standardization of in vitro stability testing of spinal implants. Eur Spine J 7: 148-54.

9. Perneger T. What's wrong with Bonferroni adjustments? 1998. Br Med J 316:1236–8.

10. Nakagawa S. 2004. A farewell to Bonferroni: the problems of low statistical power and publication bias. Behav Ecol 15(6):1044–5.

11. Kurtz S., Edidin A. 2005. Spine Technology Handbook. Burlington: Elsevier Inc; 534 p.

12. Oda I., Abumi K., Lu D., et al. 1996. Biomechanical role of the posterior elements, costovertebral joints, and rib cage in the stability of the thoracic spine. Spine 21:1423–1429.

13. Mannen E., Anderson J., Arnold P., et al. 2015. Mechanical analysis of the human cadaveric thoracic spine with intact rib cage. J Biomech 48: 2060-66.

14. Panjabi M. 2003. Clinical spinal instability and low back pain. J Electromyogr Kines 13: 371-79.

15. Pope M., Panjabi M. 1985. Biomechanical definitions of spinal instability. Spine 10: 255-56.

16. White A., Panjabi M. 1990. Clinical Biomechanics of the Spine, 2nd ed. Philadelphia: Lippincott Williams & Wilkins; 722 p.

17. Cooper C., Atkinson E., O'Fallon M., et al. 1992. Incidence of clinically diagnosed vertebral fractures: a population-based study in Rochester, Minnesota, 1985-1989. J Bone Miner Res 7.

18. Menegoni F., Vismara L., Capodaglio P., et al. 2008. Kinematics of trunk movements: protocol design and application in obese females. J Appl Biomater Biom 6: 178-85.

Figure 1. Inferior view of the interior of the rib cage, displaying the ball joint rod ends and rods threaded through the approximate centers of each vertebrae, T3-T11. The wire cable, not pictured, was then threaded superior to inferior through all of the ball joint rod ends seen.

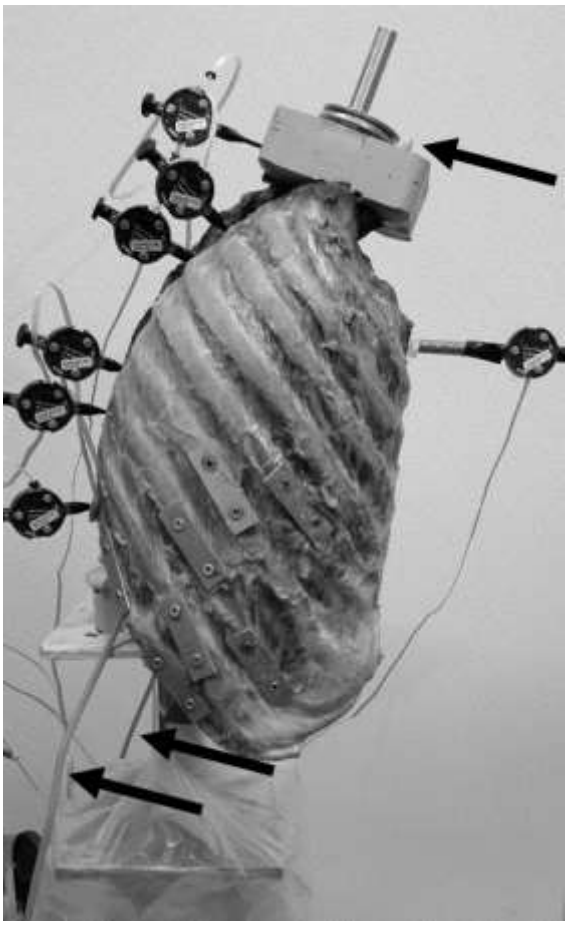

Figure 2. Sagittal view of the entire specimen, with the inferior potting mounted on the test machine. The motion tracking pins are shown at the various vertebral levels. The arrows refer to the steel wire cable, which is threaded from the superior end, through the ball joint rod ends on the interior of the rib cage, and out the inferior end of the specimen.

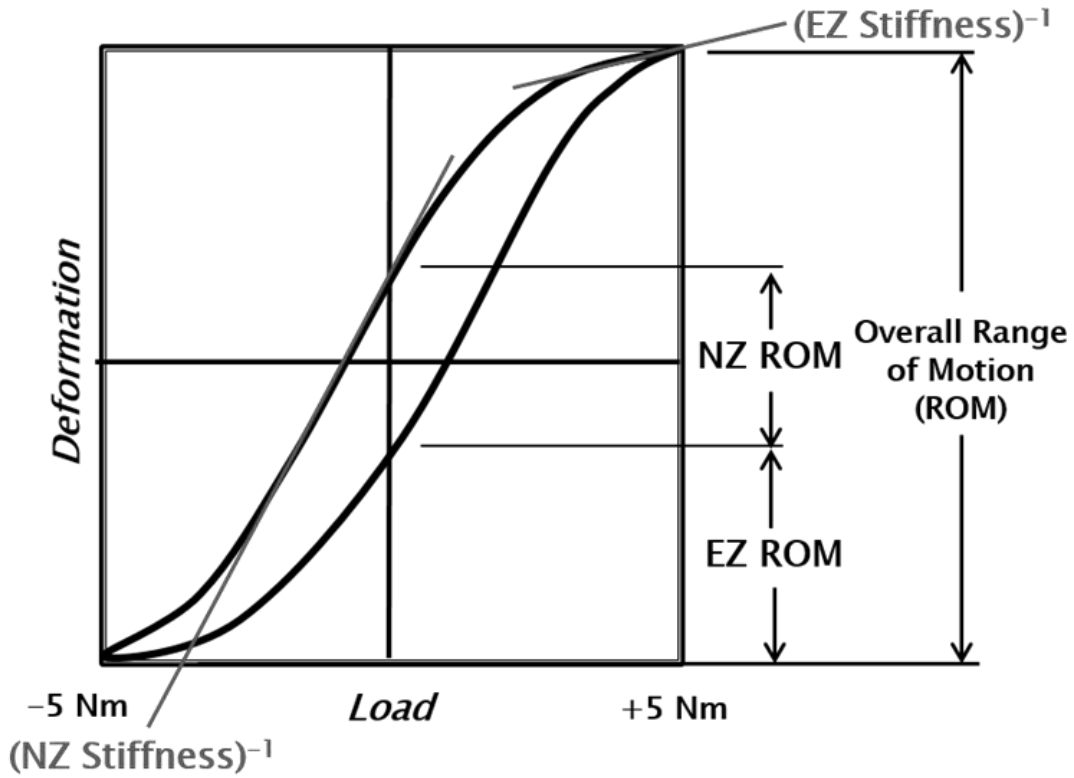

Figure 3. Deformation versus load of a typical testing cycle. The parameters of overall range of motion, elastic zone ROM, neutral zone ROM, EZ stiffness, and NZ stiffness are depicted.

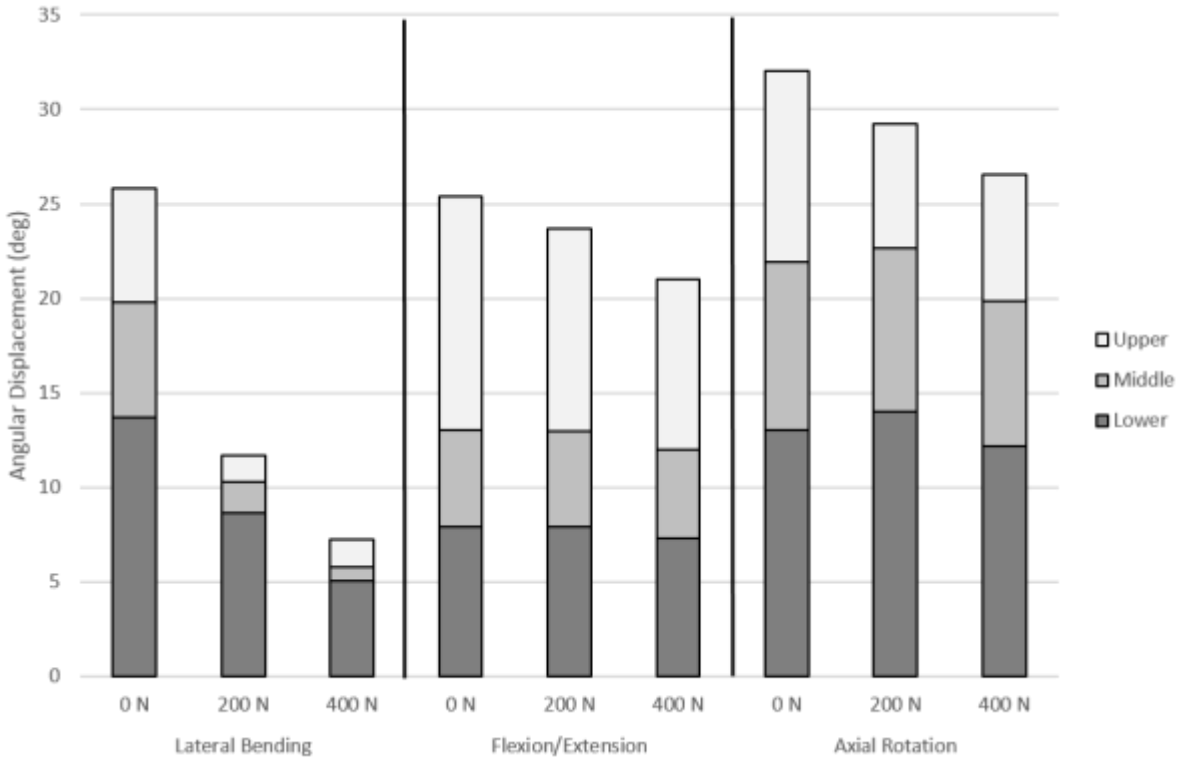

Figure 4. Mean combined segmental angular displacement range of motion values, displaying the difference between each load level and mode of bending.

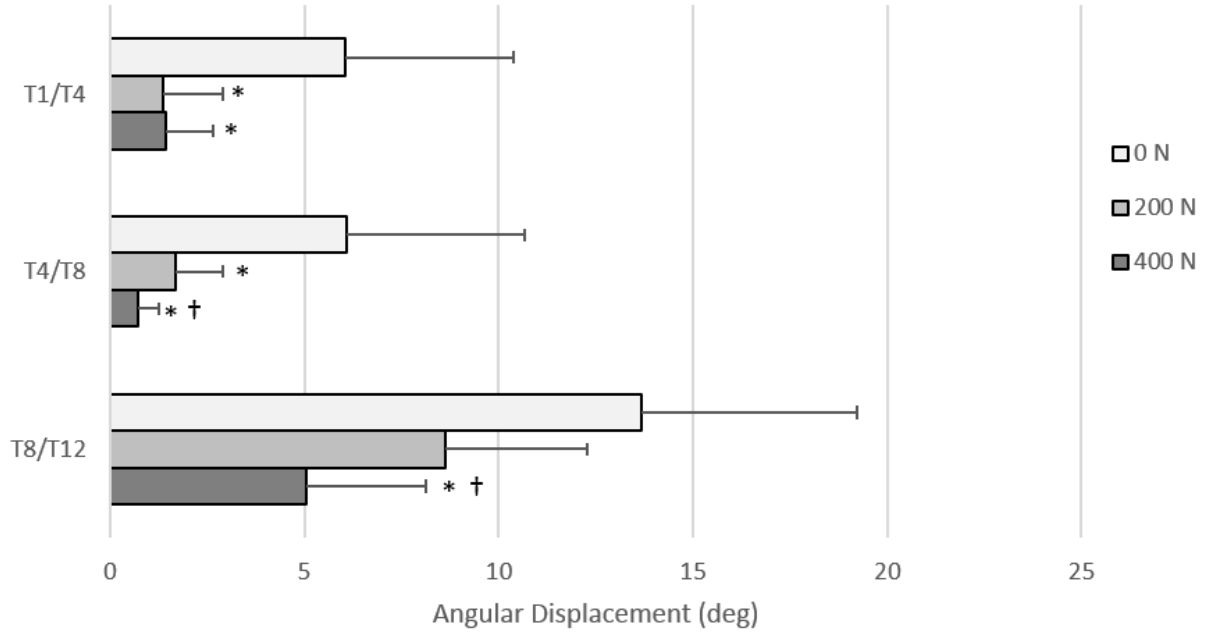

Figure 5. Mean (+ SD) segmental angular displacement range of motion values for lateral bending, comparing the baseline case of 0 N to the two other load levels, 200 and 400 N. * denotes statistically significant values between 0-200 N and 0-400 N ($p < .05$) † denotes statistically significant values between 200-400 N ($p<.05$)

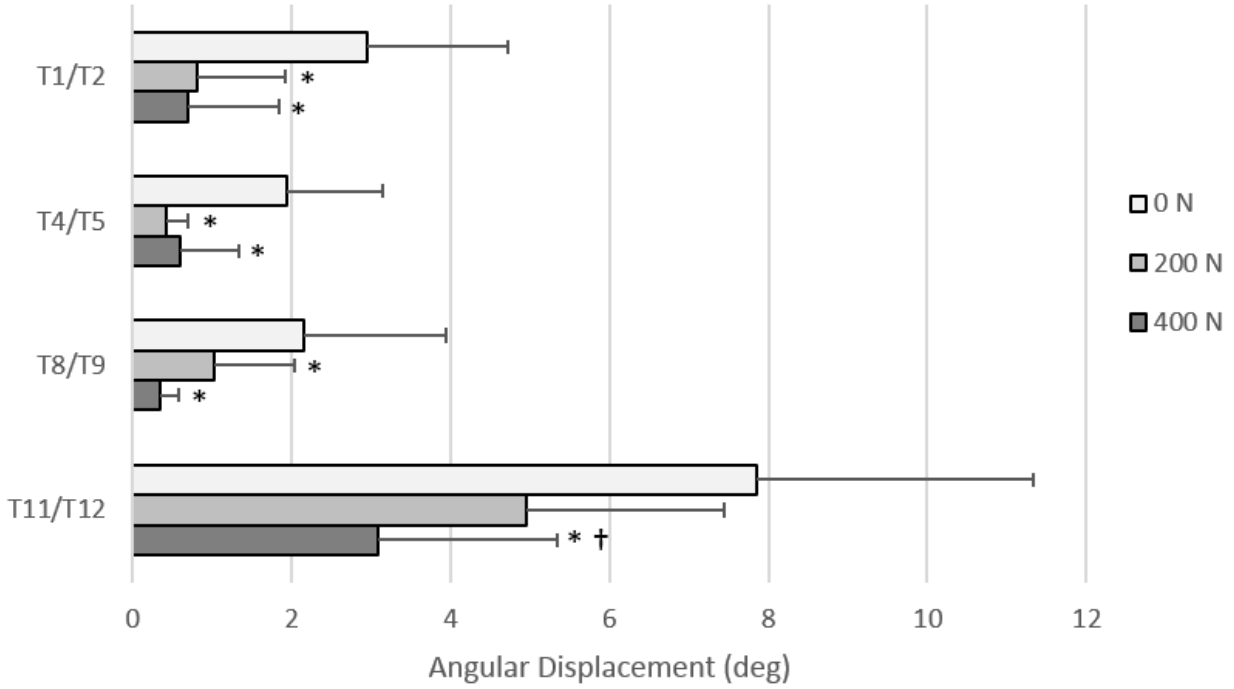

Figure 6. Mean (+ SD) individual FSU angular displacement range of motion values for lateral bending, comparing the baseline case of 0 N to the two other load levels, 200 and 400 N. * denotes statistically significant values between 0-200 N and 0-400 N ($p < .05$) † denotes statistically significant values between 200-400 N ($p<.05$)

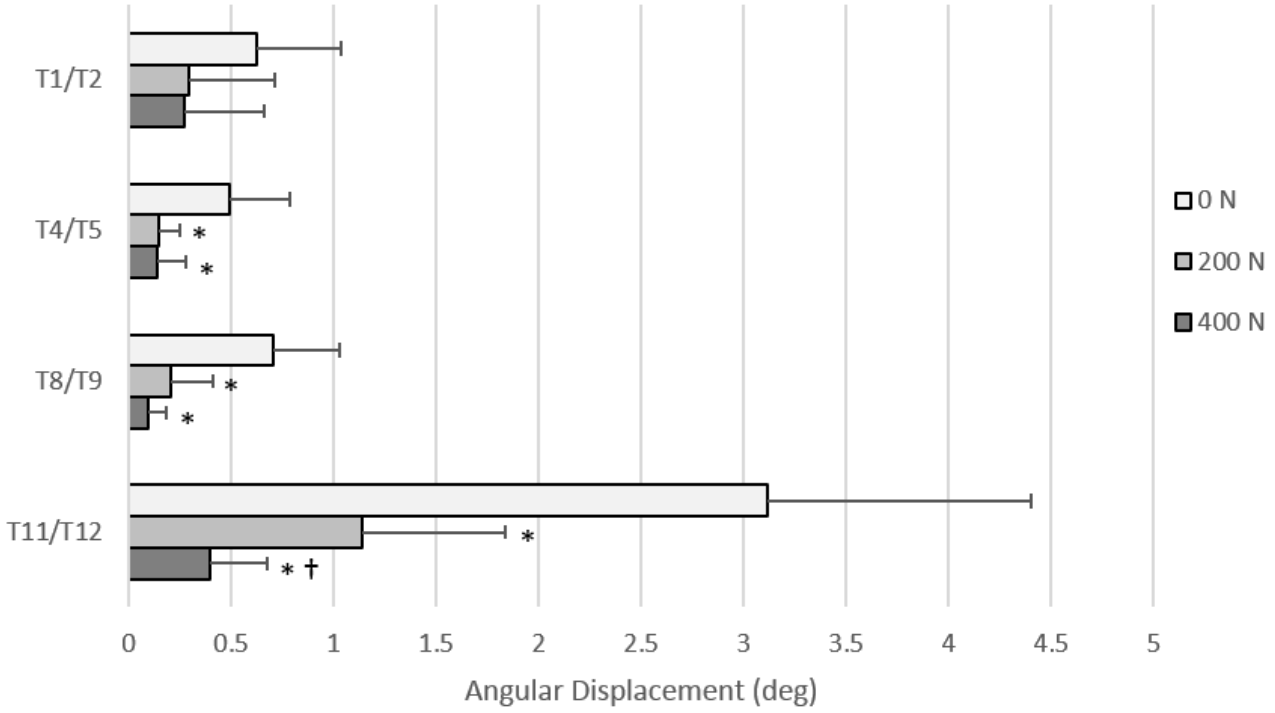

Figure 7. Mean (+ SD) individual FSU angular displacement elastic zone values for lateral bending, comparing the baseline case of 0 N to the two other load levels, 200 and 400 N. * denotes statistically significant values between 0-200 N and 0-400 N ($p < .05$) † denotes statistically significant values between 200-400 N ($p<.05$)

TABLE 1. Mean (SD) Angular Displacement Values for Individual FSU Range of Motion, Elastic Zone, and Neutral Zone

FSU Level	Load Level	Lateral Bending			Flexion/Extension			Axial Rotation			Flexion	Extension
		ROM (°)	EZ (°)	NZ (°)	ROM (°)	EZ (°)	NZ (°)	ROM (°)	EZ (°)	NZ (°)	ROM (°)	ROM (°)
T1/T2	0 N	2.96 (1.76)	0.62 (0.41)	1.50 (0.97)	7.23 (5.73)	2.70 (1.96)	2.01 (1.63)	4.76 (3.00)	1.57 (0.92)	1.02 (0.69)	4.58 (3.73)	2.79 (1.99)
	200 N	0.81 (1.11)*	0.29 (0.42)	0.29 (0.22)*	6.19 (4.37)	2.37 (1.62)	1.36 (0.86)	4.37 (1.40)	1.49 (0.42)	0.83 (0.73)*	4.19 (3.09)	1.91 (1.04)
	400 N	0.80 (1.19)*	0.27 (0.39)	0.33 (0.33)*	4.59 (3.03)†	1.72 (1.22)	0.93 (0.48)†	3.51 (1.67)	1.38 (0.64)	0.76 (0.55)	2.91 (2.14)	1.46 (0.74)*†
T4/T5	0 N	1.95 (1.21)	0.49 (0.29)	0.95 (0.85)	1.53 (1.06)	0.61 (0.44)	0.23 (0.15)	1.78 (1.37)	0.75 (0.53)	0.35 (0.27)	1.10 (0.89)	0.42 (0.21)
	200 N	0.42 (0.28)*	0.15 (0.10)*	0.32 (0.31)*	1.53 (1.57)	0.65 (0.57)	0.36 (0.40)	1.64 (0.87)	0.72 (0.40)	0.33 (0.30)	1.04 (1.21)	0.49 (0.40)
	400 N	0.60 (0.73)*	0.14 (0.14)*	-	1.49 (1.26)	0.53 (0.41)	0.44 (0.54)	1.46 (0.70)	0.63 (0.30)	0.15 (0.08)*	0.82 (0.69)	0.63 (0.55)
T8/T9	0 N	2.47 (1.68)	0.71 (0.32)	0.76 (0.93)	1.57 (1.00)	0.60 (0.33)	0.35 (0.37)	4.05 (2.32)	1.73 (0.96)	0.58 (0.48)	1.12 (0.76)	0.44 (0.25)
	200 N	1.02 (1.02)*	0.20 (0.21)*	0.78 (0.68)	1.46 (1.30)	0.47 (0.36)	0.50 (0.57)	3.03 (1.65)	1.81 (1.01)	0.80 (0.80)	0.95 (0.91)	0.48 (0.38)
	400 N	0.34 (0.24)*	0.09 (0.09)*	-	1.34 (1.27)†	0.40 (0.31)*†	0.52 (0.64)	3.72 (2.27)*	1.54 (0.78)	0.64 (0.73)	0.83 (0.85)†	0.49 (0.41)
T11/T12	0 N	7.85 (3.48)	3.12 (1.28)	1.62 (1.29)	3.90 (2.54)	1.28 (0.80)	1.28 (1.02)	3.18 (1.71)	1.37 (0.77)	0.48 (0.24)	2.62 (1.75)	1.23 (0.81)
	200 N	4.96 (2.47)	1.14 (0.70)*	2.68 (1.12)	3.98 (2.39)	1.15 (0.71)	1.62 (0.98)	3.61 (1.59)	1.46 (0.56)	0. 68 (0.68)	2.31 (1.66)	1.60 (1.06)*
	400 N	3.08 (2.26)*†	0.40 (0.28)*†	2.34 (1.76)	3.58 (2.31)	0.90 (0.50)	1.70 (1.28)	3.09 (1.32)	1.31 (0.54)	0.47 (0.45)	1.93 (1.47)†	1.58 (0.87)

* denotes statistically significant values between 0-200 N and 0-400 N ($p < .05$)

† denotes statistically significant values between 200-400 N ($p<.05$)

TABLE 2. Mean (SD) Angular Displacement Values for Segmental Range of Motion, Elastic Zone, and Neutral Zone

Segment	Load Level	Lateral Bending			Flexion/Extension			Axial Rotation			Flexion	Extension
		ROM (°)	EZ (°)	NZ (°)	ROM (°)	EZ (°)	NZ (°)	ROM (°)	EZ (°)	NZ (°)	ROM (°)	ROM (°)
Upper (T1/T4)	0 N	6.06 (4.34)	1.24 (0.87)	3.58 (2.84)	12.3 (8.09)	4.76 (3.03)	2.85 (1.99)	10.2 (5.29)	3.75 (1.88)	2.66 (1.74)	8.23 (5.60)	4.08 (2.54)
	200 N	1.36 (1.55)*	0.54 (0.55)	0.32 (0.35)*	10.8 (6.60)	4.13 (2.32)	2.38 (1.39)	6.58 (2.05)	2.89 (0.77)	1.00 (0.77)*	7.39 (4.60)	3.19 (1.55)
	400 N	1.43 (1.21)*	0.57 (0.49)	0.34 (0.23)*	9.07 (5.35)*†	3.40 (1.75)*†	2.01 (1.49)	6.69 (3.42)	2.76 (1.60)	0.94 (0.69)*	6.13 (3.52)†	2.67 (1.32)*†
Middle (T4/T8)	0 N	6.10 (4.57)	1.62 (1.15)	2.90 (2.49)	5.17 (3.27)	2.09 (1.42)	0.96 (0.60)	8.85 (6.41)	3.59 (2.96)	1.68 (1.10)	3.70 (2.50)	1.44 (0.81)
	200 N	1.67 (1.21)*	0.20 (0.19)*	1.48 (1.00)*	5.02 (3.62)	1.93 (1.38)	1.09 (0.99)	8.66 (6.16)	3.76 (2.51)	1.16 (1.20)	3.39 (2.73)	1.56 (0.95)
	400 N	0.71 (0.53)*†	0.22 (0.13)*	0.59 (0.21)*†	4.64 (3.50)†	1.70 (1.20)*†	1.13 (1.18)	7.72 (5.05)	3.48 (1.98)	0.95 (1.03)	2.90 (2.28)*†	1.63 (1.17)
Lower (T8/T12)	0 N	13.7 (5.55)	5.31 (1.54)	3.35 (2.71)	7.88 (4.36)	2.80 (1.51)	2.20 (1.58)	13.1 (3.80)	5.58 (1.76)	1.89 (1.36)	5.63 (3.28)	2.17 (1.14)
	200 N	8.62 (3.65)	1.71 (0.90)*	5.21 (2.06)	7.93 (4.64)	2.45 (1.42)*	2.89 (1.86)	14.0 (4.43)	5.89 (1.80)	2.23 (1.48)	5.07 (3.47)	2.73 (1.50)*
	400 N	5.07 (3.07)*†	0.65 (0.42)*†	3.84 (2.27)†	7.33 (4.49)	2.05 (1.07)*†	3.09 (2.34)	12.2 (3.79)	5.45 (1.48)	1.73 (1.38)	4.40 (3.12)†	2.79 (1.32)

* denotes statistically significant values between 0-200 N and 0-400 N ($p < .05$)

† denotes statistically significant values between 200-400 N ($p<.05$)

TABLE 3. Mean (SD) Stiffness Values for Individual FSU Elastic Zone Stiffness and Neutral Zone Stiffness

FSU Level	Load Level	Lateral Bending		Flexion/Extension		Axial Rotation		Flexion		Extension	
		EZS (Nm/°)	NZS (Nm/°)	EZS (Nm/°)	NZS (Nm/°)	EZS (Nm/°)	NZS (Nm/°)	EZS (Nm/°)	NZS (Nm/°)	EZS (Nm/°)	NZS (Nm/°)
T1/T2	0 N	6.30 (3.54)	3.05 (3.42)	8.96 (10.3)	1.20 (1.25)	4.75 (1.71)	1.59 (1.22)	3.63 (2.81)	1.23 (1.04)	3.06 (1.63)	1.18 (1.49)
	200 N	-	-	4.76 (7.33)	2.37 (2.77)	5.31 (1.12)	2.76 (2.63)	1.18 (0.45)	2.41 (1.80)	3.21 (1.59)	2.33 (4.14)
	400 N	-	-	6.33 (9.64)	2.26 (1.43)	5.26 (1.92)	3.43 (2.95)	2.22 (2.19)	3.14 (2.21)†	3.29 (1.90)	1.38 (0.75)
T4/T5	0 N	8.71 (4.36)	3.90 (1.73)	19.6 (8.47)	6.72 (3.92)	7.84 (3.48)	3.53 (2.44)	7.92 (4.01)	7.70 (3.83)	-	4.68 (3.27)
	200 N	-	-	9.04 (3.57)*	5.31 (3.32)	11.3 (3.38)*	4.74 (2.67)	4.51 (1.99)	7.01 (4.30)	13.6 (5.39)	3.62 (2.41)
	400 N	-	-	11.1 (5.91)*	4.13 (2.55)	6.79 (2.05)	5.77 (2.96)*†	-	5.39 (3.65)	-	2.86 (1.52)
T8/T9	0 N	8.00 (3.57)	2.92 (2.11)	30.7 (35.8)	7.22 (2.88)	7.56 (3.59)	1.72 (1.01)	8.64 (3.43)	10.6 (4.10)	-	3.82 (2.87)
	200 N	5.26 (1.56)	10.1(2.40)	43.8 (76.7)	7.39 (3.67)	5.63 (1.72)	1.82 (1.04)	6.95 (4.59)	10.4 (4.22)	14.7 (4.88)	4.35 (3.21)
	400 N	-	-	22.4 (14.4)	8.21 (4.77)	5.81 (2.56)	2.37 (1.19)*	8.83 (4.72)	11.0 (5.90)	-	5.38 (3.87)
T11/T12	0 N	3.81 (1.84)	0.73 (0.47)	9.88 (6.55)	3.97 (3.58)	4.87 (2.35)	2.18 (1.03)	7.31 (5.94)	6.10 (5.66)	8.07 (4.03)	1.83 (1.70)
	200 N	3.75 (1.79)	1.99 (1.19)*	8.23 (4.23)	2.99 (2.02)	5.71 (3.73)	2.24 (0.98)	7.43 (4.57)	4.43 (3.02)	6.84 (5.03)	1.55 (1.20)
	400 N	4.65 (4.78)	5.19 (2.76)*†	5.44 (3.31)	3.06 (1.82)	3.61 (0.93)	3.06 (1.68)†	5.41 (3.93)	4.22 (2.66)	5.47 (3.71)	1.91 (1.60)

* denotes statistically significant values between 0-200 N and 0-400 N ($p < .05$)

† denotes statistically significant values between 200-400 N ($p<.05$)

TABLE 4. Mean (SD) Stiffness Values for Segmental Elastic Zone Stiffness and Neutral Zone Stiffness

Segment	Load Level	Lateral Bending		Flexion/Extension		Axial Rotation		Flexion		Extension	
		EZS (Nm/°)	NZS (Nm/°)	EZS (Nm/°)	NZS (Nm/°)	EZS (Nm/°)	NZS (Nm/°)	EZS (Nm/°)	NZS (Nm/°)	EZS (Nm/°)	NZS (Nm/°)
Upper (T1/T4)	**0 N**	4.11 (3.11)	2.09 (2.36)	2.71 (1.66)	0.83 (0.83)	3.13 (1.79)	0.59 (0.36)	2.55 (1.92)	1.02 (1.05)	2.88 (2.56)	0.64 (0.69)
	200 N	6.90 (3.75)	5.50 (4.41)	2.32 (2.48)	0.81 (0.62)	2.57 (1.05)	1.30 (0.72)	2.07 (3.43)	1.15 (0.89)	2.57 (1.66)	0.48 (0.36)
	400 N	6.85 (2.09)	5.66 (3.84)	2.29 (1.75)	1.05 (0.62)†	3.28 (3.60)	2.94 (4.42)	1.62 (1.59)	1.43 (0.84)†	2.96 (2.11)	0.66 (0.43)†
Middle (T4/T8)	**0 N**	4.98 (4.12)	1.19 (0.74)	9.91 (8.98)	2.41 (1.58)	2.43 (0.89)	0.92 (0.59)	4.17 (3.55)	3.41 (2.34)	6.83 (4.67)	1.41 (0.86)
	200 N	5.48 (3.43)	8.13 (6.05)	6.08 (5.12)	2.80 (2.82)	3.08 (2.18)	2.19 (2.95)	3.50 (3.41)	3.91 (4.22)	6.44 (4.14)	1.69 (1.45)
	400 N	8.30 (5.50)	-	4.74 (4.10)*	3.27 (3.91)	4.51 (6.13)	2.04 (2.49)	4.69 (5.63)	2.55 (1.27)	4.79 (3.40)	2.73 (4.09)
Lower (T8/T12)	**0 N**	1.91 (0.62)	0.35 (0.16)	18.5 (40.5)	1.97 (1.73)	1.61 (0.50)	0.47 (0.33)	3.19 (3.63)	3.12 (2.84)	6.88 (5.78)	0.82 (0.68)
	200 N	1.70 (0.58)	1.20 (0.60)*	9.88 (17.0)	1.58 (1.26)	1.66 (0.52)	0.49 (0.31)	3.26 (3.61)	2.43 (2.03)	4.31 (3.43)	0.72 (0.55)
	400 N	2.87 (4.72)	3.10 (1.25)*†	2.97 (2.23)	1.79 (1.72)	2.31 (2.89)	0.59 (0.29)*	2.22 (1.73)	2.78 (3.15)	3.72 (3.35)*	0.80 (0.60)

* denotes statistically significant values between 0-200 N and 0-400 N ($p < .05$)

† denotes statistically significant values between 200-400 N ($p<.05$)

Chapter 4: Conclusions and Future Work

The research presented here has sought to better standardize the field of thoracic spine biomechanics by applying various testing aspects in tandem, in order to further understand the mechanical implications for this spinal region. Setting this work apart from past research is the presentation of all relevant parameters at various FSUs and segments, the implementation of a follower preload to allow application of forces closer to those seen in typical spinal musculature, and the inclusion of the full rib cage. The overall goal was to quantify the motion of the thoracic spine with an intact rib cage and a follower preload.

Application of a follower preload with the intact rib cage has an effect on the motion and stiffness parameters of the thoracic spine. The statistical significance of the effect varied by level and mode of bending, but overall, the combined segmental range of motion was decreased with an increase in follower load. Lateral bending had consistent statistically significant decreases in range of motion, while axial rotation had consistent statistically significant increases in neutral zone stiffness. The thoracic section of the spine with an intact rib cage was shown to withstand more physiologically reasonable weights without noticeable damage to the tissues when a follower load of up to 400 N was implemented.

Future researchers completing work in the area of thoracic spine biomechanics should aim to include an intact rib cage and a follower load in experimental setups. Better physiological characterization of the thoracic spine may be achieved if future work takes these two aspects into consideration. ROM, EZ, NZ, EZS, and NZS parameters should be included in future spine testing in order for the community to better understand the entire story of the biomechanical movement of the thoracic spine. More information about this spine region can

be compared to *in vivo* work and *in vitro* work of other spine regions if parameters are presented for various individual FSU levels and segments, as shown in this work. The data from this work could be compared to current *in vivo* thoracic spine work, in order to begin the conversation about the reliability of using cadaveric test data to make assumptions about the motion of living, healthy populations. The cadaveric experiment conducted in this study also looked at other aspects of thoracic spine testing, such as motion with a follower load and without a rib cage, changes in intradiscal pressure with and without the rib cage, influence of the floating ribs, and influence of a medical device for pediatric scoliosis. Data presented from these subsequent studies will also benefit the thoracic spine community and further characterize even more aspects of the motion of the thoracic spine.

Appendix A. Data Analysis

Calculation of motion and stiffness parameters was performed in Matlab with data files containing already synchronized load vs. displacement data from the Optotrak sensors and the ATS test machine. Exclusion criteria were applied to the parameters based upon issues with some motion sensors moving out of the bounds of the Optotrak camera, as well as some issues with resultant angular displacement values being lower than the noise of the ATS test machine.

A.1 Data Analysis Parameter Calculations Matlab Code

```
%% The purpose of this code is to calculate parameters from load v. disp
curves
%Can be used for both segments and FSUs
% Step 1: Separate data into third cycle
% Step 2: Smooth ends and middle of data
% Step 3: Find Overall ROM, NZS, NZ, EZS, and EZ for each mode of bending
% Step 4: Apply Exclusion Criteria
% Step 4: Write data to excel file
clear; clc; close all
warning('off','all')
warning
%% Data
% Determine file names:
color = ['b' 'k' 'r' 'g'];
%Define all specimen names, tests, bending modes, loads, and levels
specimen = {'FL12111534', 'IL13012749', 'IN12102967', 'MD12101843',
'MD15022062', 'PA14121034', 'MD12053191', 'FL15013190'};
test = {'Intact'};
bend = {'LB','FE','AR','AP','LR','SI'};
load = [0 2 4];
sheetname = {'T1wrtT4', 'T4wrtT8', 'T8wrtT12'}; %Segments
%sheetname = {'1', '2', '4', '5', '8', '9', '11'}; %FSUs
for specimen_num = 1:8
for test_num = 1
for bend_num = 1:3 %Corresponds to test conducted
for load_num = 1:3
%filename = [char(test) '_segment_' char(bend(bend_num)) '_'
num2str(load(load_num)) '.xls'];
filename = ['E:\Research\Harvard Study\Data\Original Parameters\'
specimen{specimen_num} '\NewData_' char(test) '_segment_'
char(bend(bend_num)) num2str(load(load_num)) '.xls'];

%% Main Program
for kk = 1:3; %each FSU or segment
% Read-in data
data = xlsread(filename,char(sheetname(kk))); %data = all load data

% Separate into one cycle
[cycle_range_up,cycle_range_dn] = Separate(data(:,7),2,5,1);

for jj = [1:6]; % Each rotation angle (FE, RL, TO) & displ (AP, RL, SI)
disp = data(:,jj); %disp = all displacement data

%% ROM Calculations (calculated for all columns of displacement data)
% Smooth data at ends:
[min_range_up,disp_min_smoothed_up,coeff_min_up,max_range_up,disp_max_smoothe
d_up,coeff_max_up] = Smooth(data(:,7), disp, cycle_range_up, 10, 2);
[min_range_dn,disp_min_smoothed_dn,coeff_min_dn,max_range_dn,disp_max_smoothe
d_dn,coeff_max_dn] = Smooth(data(:,7), disp, cycle_range_dn, 10, 2);

% Values of displacement data at -5Nm, 5Nm for up and dn cycles
neg5_up_min = coeff_min_up(1)*(-5)^3 + coeff_min_up(2)*(-5)^2 +
coeff_min_up(3)*(-5) + coeff_min_up(4);
```

```
pos5_up_max = coeff_max_up(1)*(5)^3 + coeff_max_up(2)*(5)^2 +
coeff_max_up(3)*(5) + coeff_max_up(4);

pos5_dn_min = coeff_min_dn(1)*(5)^3 + coeff_min_dn(2)*(5)^2 +
coeff_min_dn(3)*(5) + coeff_min_dn(4);
neg5_dn_max = coeff_max_dn(1)*(-5)^3 + coeff_max_dn(2)*(-5)^2 +
coeff_max_dn(3)*(-5) + coeff_max_dn(4);

ROM_up = pos5_up_max - neg5_up_min;
ROM_dn = neg5_dn_max - pos5_dn_min;
ROM_mean = (abs(ROM_up)+abs(ROM_dn))/2;

if jj==bend_num %bend_num only goes through LB, FE, AR (parameters only
calculated for those three displacement columns)
%% Neutral Zone
% Find index values of ~-1Nm and ~1 Nm within selected cycle
NZ_up_logicals = data(cycle_range_up,7)>=-1 & data(cycle_range_up,7)<=1;
NZ_up_range = (find(NZ_up_logicals == 1,1,'first') + min(cycle_range_up) -
1):(find(NZ_up_logicals == 1,1,'last')+ min(cycle_range_up) - 1);

NZ_dn_logicals = data(cycle_range_dn,7)>=-1 & data(cycle_range_dn,7)<=1;
NZ_dn_range = (find(NZ_dn_logicals == 1,1,'first') + min(cycle_range_dn) -
1):(find(NZ_dn_logicals == 1,1,'last')+ min(cycle_range_dn) - 1);

% Plot to check
%    figure(100)
%    hold on
%    plot(data(cycle_range_up,7),disp(cycle_range_up),color(load_num))
%    plot(data(cycle_range_dn,7),disp(cycle_range_dn),color(load_num))
%    plot(data(NZ_up_range,3),disp(NZ_up_range),'r-')
%    plot(data(NZ_dn_range,3),disp(NZ_dn_range),'r-')
%    plot(data(neg5_up_min,7),disp(neg5_up_min),'r-')
%    plot(data(pos5_up_max,7),disp(pos5_up_max),'r-')

% Smooth data from -1 to 1
NZ_coeff_up1 = polyfit(data(NZ_up_range,7),disp(NZ_up_range),1);
NZ_coeff_dn1 = polyfit(data(NZ_dn_range,7),disp(NZ_dn_range),1);

% NZS - Deriv of line at 0 Nm = 3rd coeffecient
NZS_up = 1/NZ_coeff_up1(1);
NZS_dn = 1/NZ_coeff_dn1(1);
NZS_mean = (abs(NZS_up)+abs(NZS_dn))/2;

% NZ
NZ = NZ_coeff_up1(2) - NZ_coeff_dn1(2);

if abs(1/NZS_dn) < .05 && abs(1/NZS_up) < .05
NZS_mean = 0;
NZS_up = 0;
NZS_dn = 0;
NZ = 0;
elseif abs(1/NZS_dn) < .05
NZS_mean = NZS_up;
NZS_dn = 0;
elseif abs(1/NZS_up) < .05
```

```
NZS_mean = NZS_dn;
NZS_up = 0;
else
NZS_mean = (abs(NZS_up)+abs(NZS_dn))/2;
end

% Neutral position
NP = (NZ_coeff_up1(2)+NZ_coeff_dn1(2))/2;

%% For FE Only - redo ROM Calculations to separate into F/E
if jj==2 %FE only
ROM_up = pos5_up_max - NP;
ROM_dn = neg5_dn_max - NP;
end

%% Elastic Zone
%EZ
if jj==2;
if ROM_up>0 %Takes care of sign (+/-) issues
    EZ_up = ROM_up - abs(NZ/2);
    EZ_dn = ROM_dn + abs(NZ/2);
else
    EZ_up = ROM_up + abs(NZ/2);
    EZ_dn = ROM_dn - abs(NZ/2);
end

else
if ROM_up>0 %Takes care of sign (+/-) issues
    EZ_up = ROM_up/2 - abs(NZ/2);
    EZ_dn = ROM_dn/2 + abs(NZ/2);
else
    EZ_up = ROM_up/2 + abs(NZ/2);
    EZ_dn = ROM_dn/2 - abs(NZ/2);
end
end
%
EZ_mean = (abs(EZ_up)+abs(EZ_dn))/2;

%EZS - Deriv of coeff equation, at load = +/-5Nm
EZS_up = 3*coeff_max_up(1)*(5)^2 + 2*coeff_max_up(2)*(5) + coeff_max_up(3);
%slope
EZS_dn = 3*coeff_max_dn(1)*(-5)^2 + 2*coeff_max_dn(2)*(-5) + coeff_max_dn(3);
%slope

EZS_up = 1/EZS_up; %stiffness
EZS_dn = 1/EZS_dn; %stiffness
EZS_mean = (abs(EZS_up)+abs(EZS_dn))/2;

else
NZ=0;NZS_up=0;NZS_dn=0;NZS_mean=0;EZ_up=0;EZ_dn=0;EZ_mean=0;EZS_up=0;EZS_dn=0
;EZS_mean=0;
end
%Code Check - Application of Exclusion Criteria
%First, we check for ROM being smaller than machine
%noise
```

```
if abs(ROM_mean) < .5
EZS_up = 0;
EZS_dn = 0;
EZS_mean = 0;
NZS_up = 0;
NZS_dn = 0;
NZS_mean = 0;
else
end
%Second we check the ends of the EZS for flatlining
if abs(1/EZS_up) < .05 && abs(1/EZS_dn) < .05 %Both ends bad, we eliminate it
entirely
ROM_up = 0;
ROM_dn = 0;
ROM_mean = 0;
EZS_up = 0;
EZS_dn = 0;
EZS_mean = 0;
EZ_up = 0;
EZ_dn = 0;
EZ = 0;
elseif abs(1/EZS_up) < .05
%Note if one end is bad we must find the displacement
%at a load of zero so that we can simulate the good
%side and mirror it. UP refers to the line on top and
%DN refers to the line on bottom.
%Locate where the data is greater than zero (or less
%than)
if jj == 2
EZS_up = 0;
else
loc_zero_dn = find(data(NZ_dn_range,7) < 0,1);
loc_zero_up = find(data(NZ_up_range,7) > 0,1);
%Now find the actual zero (the index)
zero_cross_dn_loc = NZ_dn_range(loc_zero_dn);
zero_cross_up_loc = NZ_up_range(loc_zero_up);
zero_dn_displacement = data(zero_cross_dn_loc,jj);
zero_up_displacement = data(zero_cross_up_loc,jj);
%zero_mean is the "center" point of the plot
zero_mean = (zero_dn_displacement + zero_up_displacement)/2;
ROM_half_dn = disp_max_smoothed_dn(end,1);
ROM_up = 0;
ROM_mean = abs(abs(ROM_half_dn)-abs(zero_mean))*2;
EZS_mean = EZS_dn;
end


elseif abs(1/EZS_dn) < .05 %Repeat similarly for dn if dn is the bad data
if jj == 2
EZS_dn = 0;
else
loc_zero_dn = find(data(NZ_dn_range,7) < 0,1);
loc_zero_up = find(data(NZ_up_range,7) > 0,1);
%Now find the actual zero (the index)
zero_cross_dn_loc = NZ_dn_range(loc_zero_dn);
zero_cross_up_loc = NZ_up_range(loc_zero_up);
```

```
zero_dn_displacement = data(zero_cross_dn_loc,jj);
zero_up_displacement = data(zero_cross_up_loc,jj);
%zero_mean is the "center" point of the plot
zero_mean = (zero_dn_displacement + zero_up_displacement)/2;
ROM_half_up = disp_max_smoothed_up(end,1);
ROM_dn = 0;
ROM_mean = abs(abs(ROM_half_up)-abs(zero_mean))*2;
EZS_mean = EZS_up;
end
else
end

%Write Data to Excel Files
header2save = {'Rotation','ROM up','ROM dn','ROM','NZ','NZS up','NZS
dn','NZS','EZ_up','EZ_dn','EZ','EZS up','EZS dn','EZS'};
data2save = [bend(jj),ROM_up,
ROM_dn,ROM_mean,NZ,NZS_up,NZS_dn,NZS_mean,EZ_up,EZ_dn,EZ_mean,EZS_up,EZS_dn,E
ZS_mean];
filename2write = [char(specimen(specimen_num)) char(test(test_num))
char(bend(bend_num)) '_' num2str(load(load_num)) 'segment_Parameters.xls'];
xlswrite(filename2write,header2save,char(sheetname(kk)));
line2write = ['A' num2str(jj+1)];
xlswrite(filename2write,data2save,char(sheetname(kk)),line2write);
end
end
end
end
end
end
```